Spatial and temporal variations of base cation release from chemical weathering on a hillslope scale

Erlandsson, M.[1], Oelkers, E.H.[2], Bishop, K[1], Sverdrup, H.[3], Belyazid, S.[4], Ledesma, J[5]. and Köhler, S.J.[5]

[1] Department of Earth Sciences, Uppsala University, Villavägen 16, 752 36 Uppsala, Sweden

[2] Earth Sciences, University College London, Gower Street, WC1E 6BT, London, UK

[3] School of Engineering and Natural Sciences, University of Iceland, Tæknigarður, Dunhagi 5, 107 Reykjavík, Iceland

[4] Centre of Environmental and Climate Research, Lund University, Sölvegatan 37 223 62, Lund, Sweden

[5] Department of Aquatic Sciences and Assessment, Swedish University of Agricultural Sciences, Box 7050, 750 07 Uppsala, Sweden

Highlights

- Base cation release rates from mineral dissolution was calculated for a boreal forested hillslope.
- Different models for mineral dissolution rates distributed base cation release differently over the hillslope.
- The organic-rich near-stream zone contributed significantly to the total base cation release.
- The unsaturated and the saturated zones contributed approximately equally to base cation release.
- Mass balance calculations indicate that the calculated release of Na^+ and K^+ was overestimated.

Abstract

Cation release rates to catchment runoff from chemical weathering was assessed using an integrated catchment model that included the soil's unsaturated, saturated and riparian zones. In-situ mineral dissolution rates were calculated in these zones as a function of pH, aluminum and dissolved organic carbon (DOC) concentrations along a hillslope in Northern Sweden with ten years of soil water monitoring. Three independent sets of mineral dissolution equations of varying complexity were used: *PROFILE*, *Transition-State Theory* (TST), and the *Palandri & Kharaka* database.

Normalization of the rate-coefficients was necessary to compare the equations, as published rate-coefficients gave base cation release rates differing by several orders of magnitude. After normalizing the TST- and Palandri & Kharaka-rate coefficients to match the base cation release rates calculated from the PROFILE-equations, calculated Ca^{2+} and Mg^{2+} release rates are consistent with mass balance calculations, whereas those of Na^{+} and K^{+} are overestimated. Our calculations further indicate that a significant proportion of base cations are released from the organic soils in the near-stream zone, in part due to its finer texture. Of the three sets of rate equations, the base cation release rates calculated from the normalized TST-equations were more variable than those calculated using the other two sets of equations, both spatially and temporally, due to its higher sensitivity to pH. In contrast, the normalized Palandri & Kharaka-equations were more sensitive to variations in soil temperature.

Keywords: mineral dissolution kinetics, PROFILE, Transition-State-Theory, PHREEQC, acidification, riparian zone

1. Introduction

With levels of acid rain declining for the last 30 years over large parts of the Northern hemisphere (Futter et al. 2014), academic research has turned much of its focus away from soil acidification processes. Nevertheless, intensified forestry may cause soil acidification through the long-term removal of base cations (Iwald et al. 2013). The dissolution of minerals in forest soils by chemical weathering is one of the main sources of base cations, with deposition being the other (Akselsson et al. 2007b). Quantifying base cation supply to soils is essential to determine the maximum sustainable rate of forest harvesting (Klaminder et al. 2011).

Base cations have the dual role of being both plant nutrients, and soil waters buffers against acidification. Chemical weathering rates have been extensively studied on the plot scale, and especially in the unsaturated rooting zone (Blum et al. 2002, Gerard et al. 2008). In contrast, efforts to model weathering processes on a catchment scale have rarely been undertaken, with a few exceptions (i.e. Godderis et al. 2006). To quantify weathering as a source of the buffering capacity for catchment runoff, an integrated catchment or hillslope model is required, taking account of weathering in the saturated and riparian zones, as well as in the unsaturated zone. As water moves through the hillslope it will be exposed to different chemical environments. In boreal catchment till soils, the pH will gradually increase as water moves through the soil, and then rapidly decrease in the riparian soil due to the high concentrations of organic acids associated with histosol soils. Aluminum concentrations co-vary with pH, and differ by several orders of magnitude in different parts of the hillslope (Cory et al. 2007). Carbon dioxide pressure increases with soil depth, and also increases with the organic carbon content. Each of these factors affect the mineral dissolution rates in different ways.

A complete model of base cation fluxes in a catchment is a major undertaking that includes coupling a complete hydrological description with a complete biogeochemical model that includes the role of vegetation in recycling and altering the soil chemical environment. This study is focused on defining the mineral dissolution rates in three distinct areas of catchments – the unsaturated zone, the saturated zone

which can comprise a large volume of soil between the rooting zone and the riparian zone, as well as the riparian zone itself. This is volumetrically smaller but has great potential to influence the chemistry of aquatic ecosystems since it is the final soil zone passed by much of the water prior to entering the stream.

All of the major mineral dissolution rate models are based on similar or even the same laboratory studies so they might be expected to provide relatively similar predictions. Nonetheless, choice of dissolution model approach chosen is critical to the computed chemical evolution in a soil system. Therefore in our effort to define the base cation release in different regions of a hillslope, we compared the mineral dissolution and base cation release rates calculated using three distinct mineral dissolution rate models, referred to herein as: PROFILE (Sverdrup 1990, Warfvinge and Sverdrup 1992, Sverdrup and Warfvinge 1993, Warfvinge and Sverdrup 1995), Palandri & Kharaka (Palandri and Kharaka 2004) and the TST-models (Oelkers et al. 1994, Oelkers 2001, Schott et al. 2009). In all these models, mineral dissolution rates are calculated from aqueous solution chemistry and temperature. While they all are based in part on Transition-State-Theory (Lasaga 1981, Aagard and Helgeson 1982), their respective formulation of mineral dissolution kinetics differ. The models are of varying complexity, where the rates of the Palandri & Kharaka equations are functions of pH alone, the rates from the TST-equations are functions of pH and the activities of one or more inhibiting cations, and the PROFILE equations are functions of pH, CO_2-pressure, DOC-concentrations, aqueous Al^{3+}- and base cation-activity.

The application of the three dissolution rate models will be compared based on calculations of the base cation flux in the soil waters of a small catchment located in the Krycklan Catchment Study in Northern

Sweden (Laudon et al. 2013). This site was chosen because it contains three clearly identified soil zones: 1) an upslope, mineral soil, 2) a transition zone, and 3) an organic-rich riparian soil (Oni et al. 2013). Soil water chemistry has been sampled at different depths (both unsaturated and saturated) on soil profiles from each of these zones for ten years. As such this site provides the opportunity to rigorously test the distinct dissolution rate models against long-term observations providing insight into the overall rates of base cation supply from the soil minerals to the soil waters and ultimately the watercourse draining this catchment.

2. Material & Methods

2.1 Site description and data

2.1.1 Site description

The study site is located in Northern Sweden (64°14'N, 19°46'E), 60 km inland from the Baltic Sea at an elevation of 250 m.a.s.l. The hillslope is located on the Västrabäcken stream within the Krycklan Catchment Study (Laudon et al. 2013), approximately 80 m perpendicular from the water divide. The average slope is ~3 %. The vegetation cover consists of a mature coniferous forest of Scots pine (*Pinus sylvestris*) and Norway spruce (*Picea abies*). The soil consists of glacial till, and can mostly be classified as an iron podzol, except close to the stream channel where it is classified as histosol. A more detailed site description is provided by Cory et al. (2007).

2.1.2 Soil water chemistry data

The soil water chemistry was monitored on three soil profiles along the hillslope located 4, 12 and 22 m from the stream channel along the topographic fall line. These profiles are denoted as S4, S12 and S22, respectively (Fig. 1). Each profile was monitored at 6 to 7 depths, from 5 to 90 cm below the soil surface. Soil water data was collected and analyzed from 1 to 15 times annually from 2004 to 2012. The median number of total samples was 53 per site over the nine years of sampling. Sampling was less frequent during autumn and winter; 30 % of the samples were collected from September to March. Sampling was more frequent during the spring and summer months; 70 % of the samples were collected from April to August. Soil water samples were analyzed for the concentrations of major base cations (Ca^{2+}, Mg^{2+}, K^{+}, Na^{+}), SO_4^{2-}, Cl^{-}, total Si, total Al and DOC. pH was only measured in samples collected after 2008 (Table S1). DOC was often sampled on different dates and slightly less frequently than the other constituents.

Outliers were removed from this dataset if they fulfilled the criteria:

——— (eq. 1)

Where [*X*] is the concentration of an aqueous species, μ[X] is the mean value of [X] and σ[X] is the

116 standard deviation of [X] for the site in question. The test was performed with respect to all sampled
117 solutes, and the base cation to Al-ratio. In total, 18 of 1095 samples were discarded.

118 Soil water chemistry samples were then averaged over each season, defined as: winter (December-April),
119 spring (May-June), summer (July-August) and autumn (September-November). As sampling was
120 irregular, especially for the first three years, gaps in the time series were filled using an ANCOVA-model,
121 with time as the covariate variable and season as the category variable. Missing values were then
122 calculated as:

123 (eq. 2)

124 where x_1, x_2 and x_3 are site-specific ANCOVA coefficients. For the site S22-75 cm, summer and autumn
125 seasons were lumped as only one sample was taken during autumn.

The pCO_2 of the soil waters were assumed to be time independent and were estimated from the temporal average of measurements reported by Leith et al. (2015). These authors measured pCO_2 continuously over one year (October 2012 – September 2013) at depths of 35 and 65 cm, 4 and 15 m from the stream along the same transect as the samples described above. These samples were assumed to correspond to the S4 and S12 sites, respectively. The pCO_2 as a function of depth was estimated from the linear extrapolation of measured pCO_2-values at depth from 35 to 65 cm. At shallower depths pCO_2 was assumed to be equal to that measured at 35 cm.

No data on carbon dioxide were available for profile S22. In the absence of data, the pCO_2 for the upper organic layer (6 cm) and the deepest observation point (90 cm) were estimated from measurements of the podzol profiles in a neighboring catchment (Magnusson, unpublished data), using the methods described in Magnusson (1989). The pCO_2 was assume to decrease linearly with depth from 6 to 90 cm (Table S1).

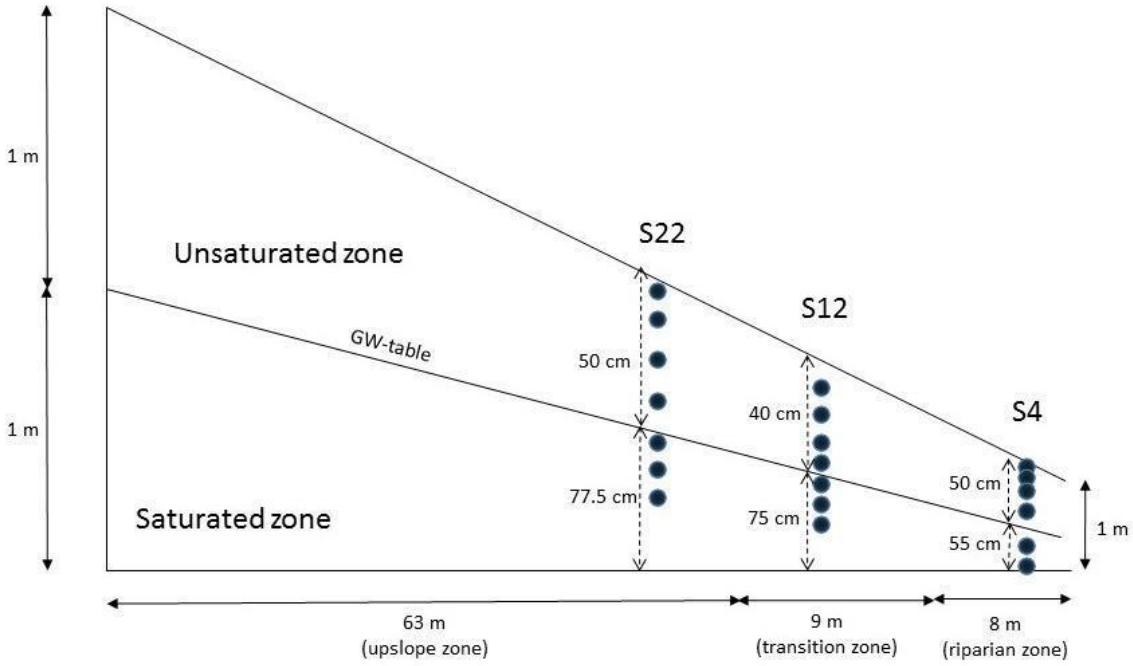

Figure 1: Schematic figure of the hillslope with the three sampled profiles (not to scale). Profile S4 represents the riparian zone, profile S12 represents the transition zone, and profile S22 represents the upslope zone. The boundary between the unsaturated and saturated zones is defined by the average

groundwater table. The bottom boundary of the hillslope is defined by the zero weathering rate depth.

2.1.3 Physical soil parameters and mineralogy

Porosity (Ø), soil texture, mineralogy and LOI (loss-on-ignition) were linearly interpolated for sites where no measurements were made. Porosity and texture were not measured for the shallower layers of S4 and S12 which were comprised largely of organic matter (peat). For the uppermost layers of these profiles (S4-10 cm and S12-5cm), the porosity was set equal to that of S4-35 cm (81 %), and the texture was set equal to that of the organic layer of S22 (S22-6 cm) (see Table S2).

The mineralogy of the transect was estimated by combining an X-Ray Diffraction (XRD) analysis, the analytical "Uppsala model" (Sverdrup and Warfvinge 1995, Sverdrup et al. 1995, Sverdrup 1996), and

information from Miskovsky (1987). The results from the XRD-analysis were used to define the abundance of quartz, plagioclase and K-feldspar. The abundance of minor minerals were obtained from the Uppsala model (Sverdrup and Warfvinge 1995), which estimates mineralogy from an analysis of the total element content of the soil. The Uppsala model was constrained so that the proportions of quartz, plagioclase and K-feldspar were equal to that obtained from the XRD-analysis, assuming that the only other minerals present were: hornblende, biotite, apatite and pyroxene (Miskovsky 1987). Quartz does not contribute to base cation release and was therefore not included in the calculations (Table S3).

Soil temperatures were not measured during the 2004-2012 study period. Instead, to estimate the seasonal variability and temperature sensitivity of base cation release rates, soil temperatures measured between 1995 and 2002 were used. The mean soil temperature was calculated for each season and site by averaging daily measurements taken over the whole period.

2.2 Dissolution rate equations

The mineral specific dissolution rates can generally be written as:

(eq. 3)

where r stands for the surface area normalized dissolution rate for the specific mineral, $F_1(A)$ denotes a chemical affinity function and r_+ stands for the forward reaction rate. The latter is often written as a sum of parallel reactions, each term representing the reaction with one dissolution agent (i.e. H^+, H_2O, OH^-, CO_2 or organic anions [R^-]):

(eq. 4)

where $r_{+,i}$ stands for the forward dissolution rate of the ith reaction, and is a function of the surrounding fluid chemistry and $F_i(T)$ represents a temperature function for the ith reaction. All symbols used in eqs. 3-15 are explained in Table 1.

Table 1: Parameters used to calculate specific mineral dissolution rates

Parameter	Symbol	Unit
Specific mineral dissolution rate per mineral surface area	r	$eq \cdot yr^{-1} \cdot cm^{-2}$
Total forward reaction rate	r_+	$eq \cdot yr^{-1} \cdot cm^{-2}$
Forward rate for the *i*:th reaction	$r_{+,i}$	$eq \cdot yr^{-1} \cdot cm^{-2}$
Rate coefficient for the *i*:th reaction	k_i	$eq \cdot yr^{-1} \cdot cm^{-2}$
Activation energy for the *i*:th reaction	$[E_A]_i$	$J \cdot mol^{-1}$
Universal gas constant	R	$J \cdot K^{-1} \cdot mol^{-1}$
Temperature	T	K
Temperature for which k_i is given	T_0	K
Mineral specific exponents in the PROFILE equations	i, j, p, q, r, s	unitless
Mineral specific exponents in the Palandri/Kharaka equations	u,v	unitless
Activity of ion *X* above which inhibition becomes significant	$\{X\}_{lim}$	unitless
Inhibiting cation with charge *m* in the TST equations	$\{C^{m+}\}$	unitless
Mineral specific exponent in the TST equations	$1/n$	unitless
Equilibrium coefficient for the formation of the precursory complex	K^*	unitless
Chemical affinity	A	$J \cdot mol^{-1}$
Ion activity product	Q	unitless
Equilibrium coefficient for mineral dissolution	K	unitless
Stoichiometric fraction of the *i*:th mineral of a solid solution	γ_i	unitless

2.2.1 Dissolution rate equations in the PROFILE model

Forward dissolution rates in this model are quantified as the sum of four terms (Sverdrup 1990, Warfvinge and Sverdrup 1992, Sverdrup and Warfvinge 1993, Warfvinge and Sverdrup 1995), in accord with:

(eq. 5)

where the f terms in the denominators correspond to mineral specific functions representing inhibition from aluminum, base cations and organic anions. The exponent for organic anions, $\{R^-\}$, was equal to 0.5 for all minerals. The functions f_H and f_{H2O} are given by:

(eq. 6)

The reaction with organic anions is self-inhibited for high concentrations of R^-, according to:

(eq. 7)

where the exponent 0.5 is equal for all minerals, whereas $\{R^-\}_{lim}$ is mineral specific. f_{CO2} is assumed to be equal to one for all minerals. All values for the mineral-specific model parameters can be found in table S4.

191

192 *2.2.2 Dissolution rate equations in the Palandri & Kharaka model*

193 The dissolution rates within the Palandri & Kharaka (2004) model are assumed to be the sum of three
194 terms, describing reactions with aqueous H^+, H_2O and OH^-. The latter reaction is however equal to zero
195 for the majority of the minerals considered for this study. Forward dissolution rates are computed from:

196 (eq. 8)

197 In contrast to the PROFILE dissolution rate equations, there are no inhibiting factors in the Palandri &
198 Kharaka equations. Thus, there is no influence from aqueous Al^{3+} or organic acids on rates according to
199 this model, except for indirect effects through pH. All values for the mineral-specific model parameters
200 can be found in table S5.

201

202 *2.2.3 Dissolution rate equations in the TST-model*

203 Forward dissolution rates based on the Transition-State-Theory (TST) model are usually written in the
204 form (Schott et al. 2009):

205 (eq. 9)

206 where $\{C^{m+}\}$ is the activity of a cation C with charge m (commonly Al^{3+}, but Mg^{2+} or Ca^{2+} for some
207 minerals). The exponent *1/n* is sometimes theoretically derived and sometimes fitted to experimental data.
208 Under a wide range of chemical conditions, i.e. when the mineral is not very far from equilibrium and the
209 surface is not saturated with precursor complexes, this equation reduces to (Schott et al. 2009):

210 (eq. 10)

211 In this study, we assume that the conditions for using the simplified eq. 10 are fulfilled.

212 Mineral-specific equations and model parameters can be found in table S6. The equation for dissolution of
213 K-feldspar was taken from Gautier et al. (1994), of pyroxene from Oelkers and Schott (2001), of apatite
214 from Harouiya et al. (2007), of plagioclase from a study on albite by Oelkers et al. (1994). The equation
215 for dissolution of biotite was taken from a study on muscovite by Oelkers et al. (2008), and fitted to data

from Taylor et al. (1999). The dissolution equation for hornblende was fitted to data from Frogner and Schweda (1998) and from Golubev et al. (2005) (see Supplementary information for details).

2.2.4 Temperature dependence of mineral dissolution rates

All three rate models employ an Arrhenius function to describe the effect of temperature on rates. *F(T)* can be written as the difference between the Arrhenius functions at two different temperatures:

——— – — (eq. 11)

For the PROFILE, T_0 is equal to 8 °C and for Palandri & Kharaka it is equal to 25 °C. For the TST-equations, T_0 was set to the temperature for which the respective dissolution experiment was conducted, or arbitrarily for minerals for which the experiments were conducted over a range of temperatures (Table S6).

227

228 *2.2.5. Dependence of dissolution rates on chemical affinity*

229 The dissolution rate models have distinct approaches to calculate the dependence of rates on chemical
230 affinity. For the PROFILE equations, there is no explicit dependence on chemical affinity (i.e. $F_1(A) = 1$).
231 Instead, the inhibition from BC and Al^{3+} (f_H and f_{H2O}, see eq. 6) are assumed to bring dissolution rates
232 close to zero near equilibrium.

233 The Palandri & Kharaka and the TST models build on the identity:

234 – (eq. 12)

235 In Palandri & Kharaka (1994), $F_1(A)$ is written as:

236 – (eq. 13)

237 where the exponents *b* and *d* are commonly set equal to unity.

238 For the TST-equations, $F_1(A)$ includes Temkin's coefficient (σ):

239 ——— = – (eq. 14)

240 The structural formulas for the minerals may differ between different databases and studies. For
241 consistency, we used the formulas found in the PROFILE database for all calculations. The structural
242 formulas, equilibrium coefficients and Temkin's coefficients are found in Table S8. For some minerals, no
243 equilibrium coefficients were found in the literature. Plagioclase was assumed to be a perfectly mixed
244 solid solution of 85 % albite and 15 % anorthite, and biotite was assumed to be a perfectly mixed solid
245 solution of and of 50 % annite and 50 % phlogopite respectively. For these two minerals, the equilibrium
246 constant is assumed to be a function of the stoichiometric fraction of each mineral in the solid solution (γ)
247 described by:

248 (eq. 15)

249 For pyroxene and hornblende, no equilibrium constants were found in the literature. Instead, the chemical
250 affinity was calculated for a structurally similar mineral. For pyroxene, diopside was used and for
251 hornblende, tremolite was used.

252

253 **2.3 Calculation of mineral specific dissolution rates**

254 For each soil profile point, the specific mineral dissolution rates (D_m) were calculated for each year and
255 season. Ion activities and mineral saturation indices were calculated using PHREEQC. The Lawrence
256 Livermore National Laboratory (LLNL) database (Johnson et al. 2000) was used to define chemical
257 equilibrium constants for minerals, chemical activities and chemical equilibrium coefficients for
258 aluminum and carbonic acid. Equilibrium between Al^{3+} and $Al(OH)_4^-$ was missing from the LLNL-
259 database and was instead taken from the minteq.v4-database (Todorov et al. 2006). The acid/base-
260 properties of DOC, as well as the complexation between aluminum and organic anions, were modelled in
261 PHREEQC using the WHAM (Windermere Humic Aqueous Model, Tipping and Hurley 1992) model of

organic acids, where DOC is modelled as a distribution of eight monoprotic and twelve diprotic weak acids with different acid/base-properties and affinities for Al-complexation. The acid dissociation constants and the distribution between the different organic acid species were taken from Tipping and Hurley (1992). The equilibrium constants for aqueous Al^{3+}-organic complexes (see Table S9) were calculated from regression against an existing application of WHAM (version V) based on complexation constants for a number of metals in the open-source PHREEQC database wateq4f.dat (Ball and Nordstrom 1991). The model performance with respect to Al-speciation was evaluated using a set of lake samples with measured concentrations of inorganic and organically bound aluminum. The correlation coefficient (r^2) between modelled and measured Al^{3+} was 0.78 with an error of prediction 0.7 µM, close to the earlier published fit (Sjöstedt et al. 2010). As pH was not measured for samples taken before 2008, all fluid samples were charge balanced to obtain $[H^+]$.

All ion activities and mineral saturation indices required to calculate dissolution rates were used together with soil temperatures in the three sets of weathering equations (eqs. 5-14) to calculate the specific dissolution rates for each mineral present.

2.4 Calculations of in-situ base cation release rates

2.4.1 Mineral surface areas

The definitions of all symbols used in eqs. 16-25 are provided in Table 2. For each point in the three soil profiles, the total base cation release rate of the mineral *m* (w_m) for 1 dm^3 of soil was calculated using:

(eq. 16)

Assuming that the minerals surface areas are proportional to their volume fractions, SA_m was calculated according to:

$$SA_m = A_{min} \cdot m_{min} \cdot \varphi_m \quad \text{(eq. 17)}$$

A_{min} was calculated from the soil texture according to Warfwinge & Sverdrup (1995) using:

$$A_{min} = 0.3 \cdot \chi_{sand} + 2.2 \cdot \chi_{silt} + 8.0 \cdot \chi_{clay} \quad \text{(eq. 18)}$$

Assuming δ_{min} is equal to 2.6 $kg \cdot dm^{-3}$, m_{min} was calculated as:

$$m_{min} = \delta_{min} \cdot V_{min} \quad \text{(eq. 19)}$$

289 V_{min} was calculated from:

290 $V_{min} = V_{bulk} - V_{org}$
291 (eq. 20)

292 Using eq. 19 and the identity $LOI = m_{org}/(m_{org} + m_{min})$, eq. 20 can be rewritten as:

293 (eq. 21)

294 Finally, by replacing m_{org} with V_{org}/δ_{org}, where δ_{org} stands for the density of organic material, which was
295 assumed equal to 0.5 kg·dm^{-3}, gives

296 (eq. 22)

For any unit volume, V_{bulk} was calculated as:

$$V_{bulk} = 1 - Ø \quad \text{(eq. 23)}$$

The total base cation release rate for each site *s*, was calculated by summing the dissolution rates for each of the *n* minerals present, such that

(eq. 24)

Furthermore, average specific mineral dissolution rates were calculated for each site using:

(eq. 25)

where $SA_{min,S}$ refers to the total mineral surface area at site *s*.

Table 2: Parameters used to calculate in-situ base cation release rates.

Parameter	Symbol	Unit
Base cation release rate for mineral *m* per dm^3 soil	w_m	$eq \cdot yr^{-1} \cdot dm^{-3}$
Specific dissolution rate for mineral *m*	r_m	$eq \cdot yr^{-1} \cdot cm^{-2}$
Surface area of mineral *m* per dm^3 soil	SA_m	$cm^2 \cdot dm^{-3}$
Total field surface area per kg of minerals	A_{min}	$cm^2 \cdot kg^{-1}$
Mass of minerals per dm^3 soil	m_{min}	$kg \cdot dm^{-3}$
Mass of organic matter per dm^3 soil	m_{org}	$kg \cdot dm^{-3}$
Weight fraction for mineral *m*	ϕm	unitless
Weight fraction for soil texture class	$\chi_{texture\ class}$	unitless
Mineral density	δ_{min}	$kg \cdot dm^{-3}$
Organic matter density	δ_{org}	$kg \cdot dm^{-3}$
Total mineral volume per dm^3 soil	V_{min}	$dm^3 \cdot dm^{-3}$
Total organic matter volume per dm^3 soil	V_{org}	$dm^3 \cdot dm^{-3}$
Bulk volume per dm^3 soil	V_{bulk}	$dm^3 \cdot dm^{-3}$
Loss-on-ignition	*LOI*	unitless
Total base cation release rate for site *s* per dm^3 soil	w_S	$eq \cdot yr^{-1} \cdot dm^{-3}$
Average specific mineral dissolution rates for site s	r_S	$eq \cdot yr^{-1} \cdot cm^{-2}$

2.4.2 Calculations of hillslope base cation fluxes

The total base cation flux was calculated for each of the three soil profiles. For each profile, equidistant boundaries were drawn horizontally between the sites, so that the weathering flux from each site was taken to represent a volume of soil, V_S. All symbols used in eqs. 26-30 are defined in Table 3. The base cation flux from each soil volume was calculated from:

(eq. 26)

A lower boundary was defined as where the mineral dissolution rate is assumed to approach zero. This

lower boundary represents the effective infiltration depth of the soil profile, and was set to 1 m near the stream, and increased linearly with the distance from the stream to a depth of 2 m at the water divide 80 m from the stream (see Fig. 1). The base cation release rates calculated for the deepest sampling location of each profile (65 cm for S4, 70 cm for S12 and 90 cm for S22) were assumed to be representative down to 1 m depth, below which additional soil volumes (V_{n+1}) were assumed to be present down to the zero rate

boundary. In the V_{n+1} volumes, the mineral dissolution rates were assumed to decrease linearly with depth to zero. The total base cation flux from each profile was then calculated by summing the fluxes from all soil volumes in accord with:

(eq. 27)

The calculations of base cation release rates were upscaled to the whole hillslope by letting S22 represent the upslope zone (17-80 m), S12 represent the transition zone (8-17 m), and S4 represent the riparian zone (0-8 m from the stream). The groundwater surface lies approximately 30 cm below the surface at S4, 50 cm below at S12 and 75 cm below at S22, and was assumed to be at 1 m depth at the water divide (Amvrosiadi et al. 2016). The average depth to the zero rate depth was calculated to be 160.6 cm for the upslope zone, 115.6 cm for the transition zone and 105 cm for the riparian zone. The area specific base cation release rate from each soil zone then becomes:

(eq. 28)

The base cation release rate from a one meter wide section of the hillslope then becomes:

(eq. 29)

where subscripts *M, T* and *R* denote the mineral, transition and riparian zones respectively.

The base cation release rates were calculated for each year and season, and were then averaged over time to calculate the spatial variability of rates over the different compartments of the hillslope, i.e. the riparian/transition/upslope zones and the unsaturated/saturated zones. Sites above 30 cm at S4 and above 50 cm at S12 were assigned to the unsaturated zone. At S22, base cation release from the site at 75 cm was divided equally between the unsaturated and saturated zone. A simple analysis of temperature sensitivity was also carried out by calculating the base cation release rates for a temperature increase of 1 °C applied uniformly over the hillslope.

Table 3: Parameters used to calculate base cation release rates from the hillslope

Parameter	Symbol	Unit
Soil volume represented by site s	V_S	dm^3
Base cation release rate from soil volume V	W_V	$eq \cdot yr^{-1}$
Base cation release rate from soil profile Sx	W_{Sx}	$eq \cdot yr^{-1}$
Number of sites of profile Sx	n	unitless
Average depth to the zero rate depth for soil zone Z	dZ	m

Area of soil zone Z	A_Z	m^2
Base cation release rate from soil zone Z	W_Z	$eq \cdot yr^{-1} \cdot m^{-2}$
Base cation release rates from a 1 m wide section of the hillslope	W_{hill}	$eq \cdot yr^{-1}$

343

344 *2.4.3 Normalization of weathering rates to PROFILE equations*

345 Numerous studies have concluded that mineral dissolution rates measured in the laboratory differ by
346 several orders of magnitudes, both from one another and from field rates. In this study, however, we focus
347 on how weathering rates are distributed over the hillslope. For this reason, all mineral weathering rates
348 were normalized to those calculated from the PROFILE-model equations, as these have already been
349 applied to our study site (Sverdrup and Rosén 1998, Akselsson et al. 2007a) and are assumed to be the
350 benchmark for the element release rates of the transect.

For each mineral, the TST- and Palandri & Kharaka equations were normalized to give the same base cation release rates as calculated from the PROFILE equations. The rate coefficients of each mineral of the TST and Palandri & Kharaka equations were multiplied by a mineral-specific factor γ_{min} equal to:

——————— (eq. 30)

where $W_{hillslope}$ is the total base cation flux from the whole hillslope calculated from eq. 29, and $\gamma_{M,m}$ is the normalization factor for model M (either TST or Palandri & Kharaka) for mineral m. Rates calculated from these normalized equations will be referred to as normalized rate models in the discussion below.

2.4.4 Mass balance calculations and sensitivity of results to poorly contrained parameters

Insight into the fate of the released base cations can be obtained from consideration of the total chemical mass balance of hillslope fluxes for each cation in accord with:

$$R_{BC} + U_{BC} + L_{BC} = D_{BC} + (W_{hill})_{BC} \quad \text{(eq. 31)}$$

where R_{BC} refers to the retention, U_{BC} designates the tree uptake, L_{BC} refers to the leakage and D_{BC} represents the deposition. The relative retention of a base cation in the hillslope was calculated as:

——————— (eq. 32)

D_{BC} and U_{BC} were taken from a MAGIC (Cosby et al. 2001)application at the nearby site of Gammtratten (Zetterberg et al. 2014). L_{BC} was defined as the lateral transport flux of base cations across the S4 profile, and was calculated following the methods of Ledesma et al. (2013). This lateral transport is based on the runoff output of BC over the 10 year monitoring period. The retention term consists of contributions of ion exchange and biological uptake other than tree uptake, and closes the mass balance of the catchment.

A sensitivity analysis of calculated base cation flux was performed with respect to three poorly constrained parameters:

1. Hillslope geometry and zero rate depth: Calculations were carried out using two alternative values of

the zero rate depth at the water divide: 1 and 2 m.

2. Reactive mineral surface area: The calculated mineral surface area for site S22-90 was approximately three times as high as the rest of the S22 profile. Thus, calculations were performed using two alternative reactive surface area values for S22-90: 966 $m^2 \cdot kg^{-1}$ minerals as calculated from eq. 18, and 339 $m^2 \cdot kg^{-1}$ minerals, i.e. equal to that of S22-75 cm.

3. Soil moisture saturation: In PROFILE, the mineral dissolution rates are multiplied by the soil moisture saturation (θ). The calculations of the hillslope base cation release rates were performed both with and without the soil moisture factor. The soil moisture saturation (θ) was taken as the average from sub-daily TDR (Time-Domain Reflectometry) measurements Oct 2008 – Sep 2014.

With all combinations above, eight different estimates of W_{Hill} were calculated (Table S10). Combined with the three different sets of rate equations, a total of 24 estimates of W_{Hill} define the range of base cation fluxes presented here.

3. Results

3.1 Hillslope base cation fluxes

3.1.1 Normalization of the Palandri & Kharaka- and TST-equations

Before normalization of the Palandri & Kharaka- and TST-equations, the base cation release rates calculated from the three sets of equations differed by several orders of magnitude. Using the basic assumptions, the specific base cation release rates per unit of catchment area from the hillslope (W_{hill}) was estimated to be 0.14-0.27 eq[BC]·yr^{-1}·m^{-2} from the PROFILE-equations. In contrast, the TST-equations gave 150 times higher rates before normalization (26-41 eq[BC]·yr^{-1}·m^{-2}), and the Palandri & Kharaka-equations gave more than 10,000 times higher rates (1500-2900 eq[BC]·yr^{-1}·m^{-2}). The normalization factors for all minerals are given in Table 4.

Table 4: Normalization factors (γ_{min}) for the Palandri & Kharaka and the TST-equations. The factor also includes a conversion of units to [eq(BC)·cm^{-2}·s^{-1}].

Mineral	γ_{min} (Palandri & Kharaka)	γ_{min} (TST)
K-feldspar	$5.74 \cdot 10^{-2}$	$1.20 \cdot 10^{-3}$
Plagioclase	$7.85 \cdot 10^{-2}$	14.8
Pyroxene	0.82	$4.30 \cdot 10^{-3}$
Hornblende	$6.44 \cdot 10^{-3}$	3.91
Biotite	0.12	6.65
Apatite	$2.67 \cdot 10^{-5}$	$4.54 \cdot 10^{-3}$

3.1.2 Mass balance and sensitivity calculations

After normalization, the calculated base cation release rates from the hillslope is by definition identical from all three sets of equations. Sensitivity analyses were performed to assess the effects of hillslope geometry, mineral surface area and soil saturation on the computed results. Of these three factors, hillslope geometry had the greatest effect; decreasing the zero rate depth to 1 m along the whole length of the hillslope reduced the total base cation release from 0.27 to 0.19 eq[BC]·yr^{-1}·m^{-2}. In contrast, decreasing the mineral surface area of the deepest layer reduced the total base cation release to 0.21 eq[BC]·yr^{-1}·m^{-2}, and including a soil moisture factor reduced it only to 0.24 eq[BC]·yr^{-1}·m^{-2} (Table 5).

Of the 0.27 eq[BC]·yr^{-1}·m^{-2} calculated to be released according to the highest estimate, 23 % was Ca^{2+}, 15

410 % was Mg^{2+}, 56 % was Na^{+} and 8 % was K^{+}. A fraction of each was retained by the soil through ion
411 exchange, biological uptake or immobilization. This fraction was calculated to be 53 % of the Ca^{2+}, 61 %
412 of the Mg^{2+}, 83 % of the Na^{+} and 81 % of the K^{+}. Assuming the lowest estimate of base cation release of
413 0.13 eq[BC]$\cdot yr^{-1}\cdot m^{-2}$, the calculated retention was 15 % for Ca^{2+}, 30 % for Mg^{2+}, 67 % for Na^{+} and 72 %
414 for K^{+} (Table 5, Fig. 2).

415 Computed results suggest that the dissolution of distinct minerals dominated the fluxes of certain
416 elements. The flux of Na^{+} and K^{+} were each dominated by the dissolution of a specific mineral,
417 plagioclase for the case of Na^{+} and K-feldspar for K^{+}. K-feldspar was supersaturated at the two deepest
418 points of profile S22 as well as for the deepest point of the profile S12, and near to equilibrium for several
419 other of the observation points, which reduced the total K^{+}-flux substantially. The Mg^{2+}-fluxes were
420 dominated by hornblende dissolution, whereas the Ca^{2+}-flux was not dominated by the dissolution of any
421 single mineral; for Ca^{2+}, hornblende contributed to 41 % of the total flux, plagioclase 38 %, apatite 13 %
422 and pyroxene 8 %.

Table 5: Hillslope mass balance calculations (eq[BC]·yr^{-1}·m^{-2}) of base cation fluxes.

Mass balance term	Ca^{2+}	Mg^{2+}	Na^{+}	K^{+}
Deposition	0.0059	0.0027	0.0057	0.0015
Tree uptake	-0.0041	-0.0011	-0.0001	-0.0012
Leaching	-0.028	-0.016	-0.026	-0.003
Mineral dissolution	0.032-0.062	0.022-0.041	0.072-0.15	0.014-0.021
% Retention	15-53	13-61	67-83	72-81

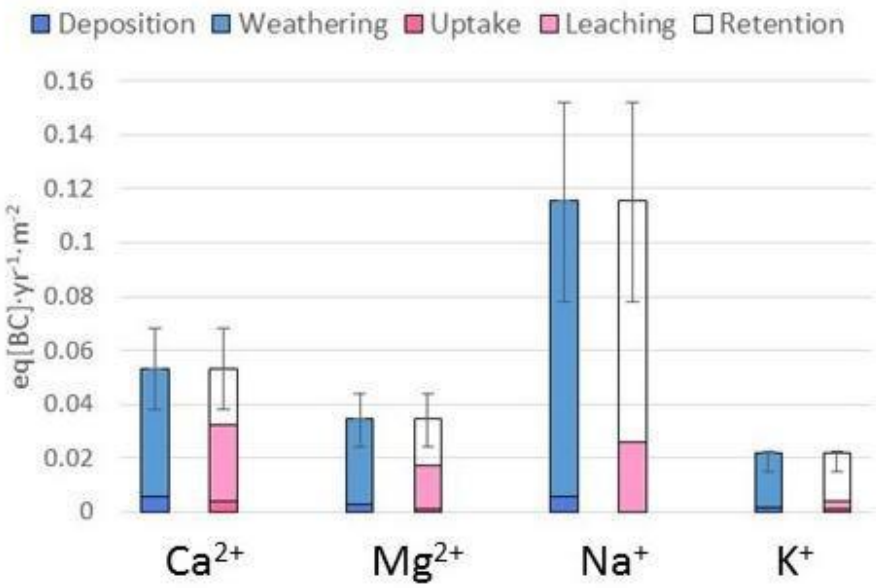

Figure 2: Mass balance calculation of base cations for the hillslope. The error bars apply to the weathering and the retention terms and are defined by the range calculated from the 24 possible combinations of dissolution rate equations and model parameters (see section 2.4.4).

3.2 Spatial variability of base cation release rates

The calculations performed in this study allow comparison of the base cation release rates of the distinct soil zones. Results suggest that the specific base cation release rates were of similar magnitude from the riparian and upslope soils (Fig. 3). However, the uncertainty in the base cation release rates from the upslope soil was much larger, because of uncertainties in the zero rate depth and the soil texture. Of the total base cation release from the hillslope, the upslope soil contributed to 49.7-80.5 %, the transition zone to 13.9-37.4 % and the riparian zone to 5.6-15.4 %. In terms of the relative contribution from the

437 unsaturated versus the saturated zones, the contribution from the former was 29.0-63.2 %, and from the
438 latter 36.8-71.0 % (Table S11).

439 The variability of specific mineral dissolution rates (r_S) over the distinct soil zones is different from that of
440 the base cation release rates, and also clearly illustrates the difference between the three sets of rate
441 equations. The mineral dissolution rates reflect the pH-gradient of the hillslope, and are thus highest in the
442 riparian zone, and lowest in the deep upslope soil. Furthermore, the variability is much more pronounced
443 when rates were calculated using the normalized TST-equations than with the normalized Palandri &

Kharaka-equations or the PROFILE-equations. The specific mineral dissolution rates of the deep upslope soil (S22-90 cm) differs from that of the shallow riparian soil by a factor of 3.3 for the PROFILE equations, a factor of 6.7 for the normalized Palandri & Kharaka equations, and a factor of 32 for the normalized TST-equations (Fig 4).

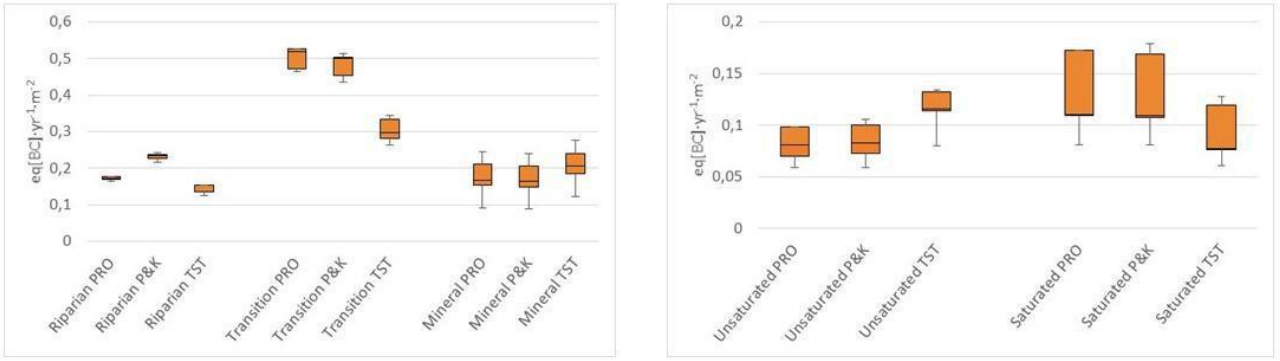

Figure 3: Distributions of base cation release rates W_Z [eq[BC]·yr^{-1}·m^{-2}] between the upslope-, transition- and riparian soils (left) and the unsaturated/saturated zones (Cosby et al.), as calculated from the PROFILE-, normalized TST- and normalized Palandri & Kharaka-equations. The median, quantiles and whiskers are defined by the five different alternative calculations (section 2.4.4).

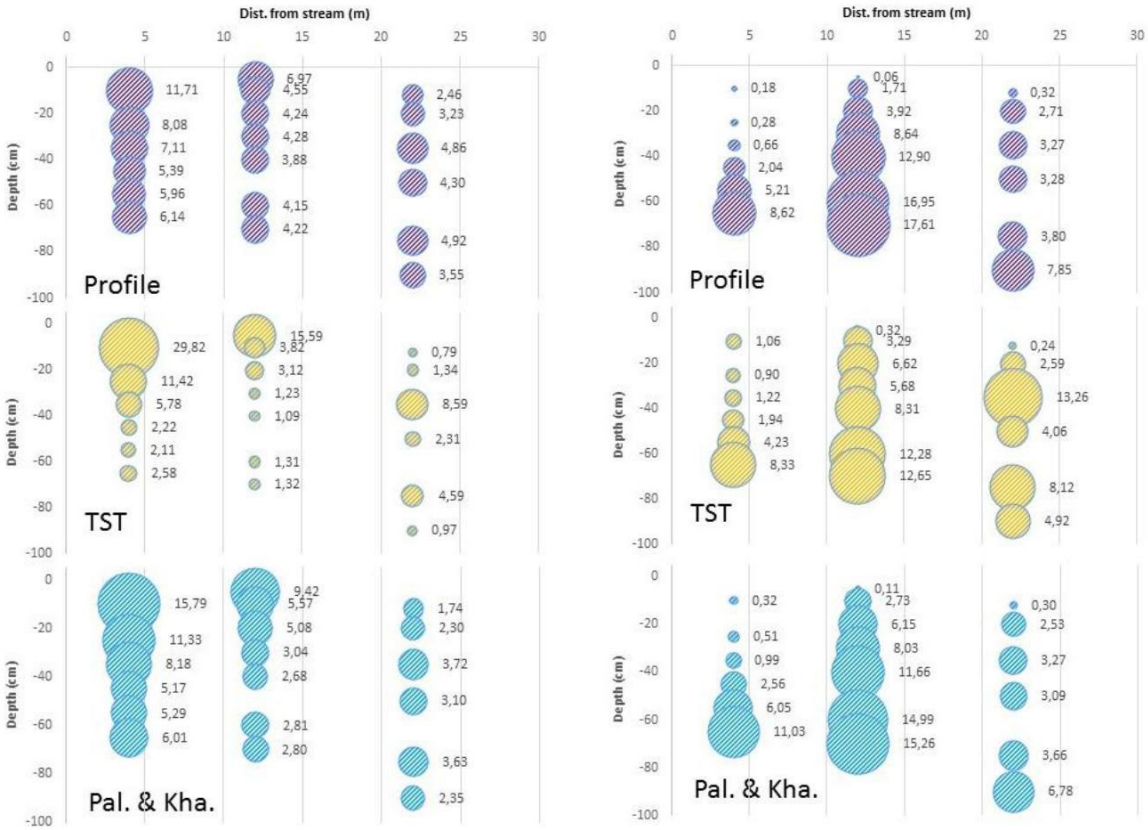

453

454 *Figure 4: Mineral dissolution rates r_S (left panel) and base cation release rates w_S (right panel) for all*

455 *depths and profiles of the transect calculated from PROFILE-equations (upper), TST-equations*

normalized to PROFILE (middle) and Palandri & Kharaka-equations normalized to PROFILE. The labels gives the relative contribution to the total area-specific weathering rates in percent.

3.3 Inter-annual variability and trends in calculated base cation fluxes

The years 2004-2012 was a period of recovery from soil acidification. Of the 19 sampling points, 14 showed a significant increase in Acid Neutralizing Capacity (ANC) and 7 showed a significant pH increase. These trends were not always linear, and the inter-annual variability was larger for a majority of the sites. The median pH increase among all sites was 0.13 units, and the median increase in ANC was 41 µeq/L.

The change in calculated base cation fluxes (W_{hill}) resulting from these decadal trends and inter-annual variations of the soil water chemistry yielded a significant decrease ($p < 0.05$) under all model assumptions when calculated using the normalized TST- or normalized Palandri & Kharaka-rate equations. When the PROFILE-equations where used, the decrease was significant under six of the eight different model assumptions. The trend in the base cation flux calculated from the TST-equations indicated a decrease of 28-36 % between 2004 and 2012. In contrast, the decrease in base cation flux from the Palandri & Kharaka-equations was 7.4-10.2 %, and from the PROFILE-equations only 2.7-4.7 % (Fig. 5).

Calculated results suggest that the decrease in base cation fluxes over the 2004 to 2012 time period were dominated by changes in the unsaturated zone, regardless of the dissolution equation or model employed (Fig. 5). The decrease calculated from the normalized TST-equations was 43-47 %, from the normalized Palandri & Kharaka-equations 14-15 %, and from the PROFILE-equations 8.6-8.8 %. No significant trends of base cation release rates from the saturated zone were calculated for any combination of equations.

Figure 5: Left: Annual time series of base cation fluxes W_{hill} calculated from the PROFILE-, normalized Palandri & Kharaka- and the normalized TST-equations respectively, using the assumptions of Model 4 (Table S10). Right: Base cation fluxes separated between the unsaturated and the saturated zones.

3.4 Seasonality and temperature sensitivity

The base cation release rates (W_{hill}) were 71 % higher during summer than during winter months when calculated from the PROFILE equations, and 120 % higher when calculated from the Palandri & Kharaka- equations. In contrast, the base cation release rates calculated using the TST-equations were highest

during the autumn months due to lower aqueous Al^{3+}-concentrations in the upslope soil; the autumn release rates were 126 % higher than those during winter months.

Increasing the temperature by one °C uniformly over the hillslope resulted in moderate increases of base cation release rates according to the PROFILE- and the TST-equations. The calculated rates increased by 8.7-9.0 % for the former and by 5.8-6.4 % for the latter. The Palandri & Kharaka-equations were much more sensitive to temperature changes, for which the calculated rates increased by 46-47 %. The temperature sensitivity is not only dependent on the activation energy, but also on the Al-speciation. As the temperature increases, the equilibrium between Al^{3+}- and OH^- shifts to higher activities of Al/OH-complexes. The calculated aqueous Al^{3+}-concentration decreased by 1-4 % in the mineral and transition zones for a temperature increase of one °C, which affected the calculated base cation release rates, especially from the TST-equations. Without the shift in Al-speciation, the temperature sensitivity of the TST-equations would have been similar to that of the PROFILE-equations, i.e. an increase in base cation release rates of around 8 %.

4. Discussion

4.1 Comparison of the dissolution rate equations

This study focused on the spatial and temporal variability of base cation fluxes from mineral weathering in a boreal forested hillslope. We found it was essential to normalize the rate-coefficients of the mineral reaction equations to compare results found using various mineral dissolution rate models. Without normalization, the three sets of equations result in dramatically different weathering estimates. As reported above, before normalization the base cation release rates calculated from the TST equations were 150 times higher than those from PROFILE, while those calculated from the Palandri & Kharaka equations were more than 10,000 times higher. This large difference is largely due to differences in the calculated dissolution rates of one or a few minerals: K-feldspar and hornblende for the TST-equations, hornblende and apatite for the Palandri & Kharaka-equations. To a large degree these differences can be attributed to the commonly described discrepancies between field- and laboratory rates (Schnoor 1990, Brantley 1992). However, the very high dissolution rates for apatite calculated from the Palandri & Kharaka-equations – up to $4 \cdot 10^{-4}$ eq[BC]$\cdot$ $yr^{-1} \cdot cm^{-2}$ [mineral surface area], or up to 60,000 times higher than rates calculated from the PROFILE equation – is difficult to explain.

The distribution of base cation fluxes over the different parts of the hillslope was similar for the PROFILE- and the normalized Palandri & Kharaka-equations, whereas the normalized TST-equations attributed more of the base cation release to the upslope soil and the unsaturated zone (see Figs. 3&4). The reason for this is the very low Al^{3+}-concentrations ($5 \cdot 10^{-9}$-$6 \cdot 10^{-10}$ M) of the upslope soil relative to the other soil zones. The response to changing pH and soil temperature were also very different between the three sets of equations. Whereas the PROFILE and the normalized Palandri & Kharaka-equations only responded moderately to a 0.13 unit pH-increase during the observed decade of recovery from acidification (2004-2013), the normalized TST-equations predicted a substantial reduction in base cation release rates from the hillslope. In contrast, an increase in soil temperatures of 1 °C was estimated to increase base cation release rates by ~10% if calculated using the PROFILE or the normalized TST-

equations, whereas those calculated using the normalized Palandri & Kharaka-equations increased by almost 50 %. Again, this increase is mostly associated with apatite due to its very high activation energy in the Palandri & Kharaka-database (250 $kJ \cdot mol^{-1}$, see Table S7). Without apatite, the calculated increase in base cation release rates would have been only ~15%. Note that while the response to pH is inherent to the model formulation, the response to temperature is only due to differences of the respective activation energies reported (Table S7), other than for the small temperature effect on aluminum speciation.

The contrasting results from the three weathering models can be understood by plotting their variation with pH and Al^{3+}-concentration. The upper panel of Fig. 6 displays the specific base cation release rates (D_m) for each mineral present at the study site, calculated from the PROFILE- and the normalized TST-equations as functions of Al^{3+}-concentration; note that dissolution rates according to the normalized Palandri & Kharaka-equations are independent of Al^{3+}-concentration. pH, DOC and BC-concentrations were held constant in these calculations, while the total aluminum concentrations were varied between $2 \cdot 10^{-7}$-$4 \cdot 10^{-5}$ M, resulting in Al^{3+}-concentrations from $5 \cdot 10^{-10}$ to $2 \cdot 10^{-5}$ M (a range similar to that found in hillslope soil water). For the PROFILE-equations, the effect of changing aqueous aluminum activity on specific base metal release rates was modest. The rates are significantly slowed by Al^{3+}-concentration only when it exceeds $5 \cdot 10^{-7}$ M, and even then base cation release rates are only inhibited slightly. In contrast, the TST-equations were more sensitive to variations in Al^{3+}-concentration (except for the Al-free minerals pyroxene and apatite), with base cation release rates varying by more than two orders of magnitude for some minerals (i.e. biotite). Furthermore, the TST-equations are sensitive to variations in $\{Al^3\}$ over the whole concentration range.

A similar plot of specific base cation release rates calculated from the three sets of rate equations as a function of pH, as shown in the lower panel of Fig. 6, illustrates why the specific rates are more variable when calculated with the TST-equations than when calculated using the PROFILE-equations. In these calculations, total Al, DOC and BC-concentrations were held constant, whereas Al^{3+}-concentration was varied with pH. Rates calculated using the PROFILE equations decrease the least with pH, the Palandri & Kharaka equations display an intermediate response, whereas the rates from the TST equations decrease the most. For the PROFILE-equations, only the base cation release from pyroxene decreased by more than one order of magnitude in response to increasing pH, whereas for the TST-equations, the base cation release decrease by at least one order of magnitude for all minerals except for pyroxene.

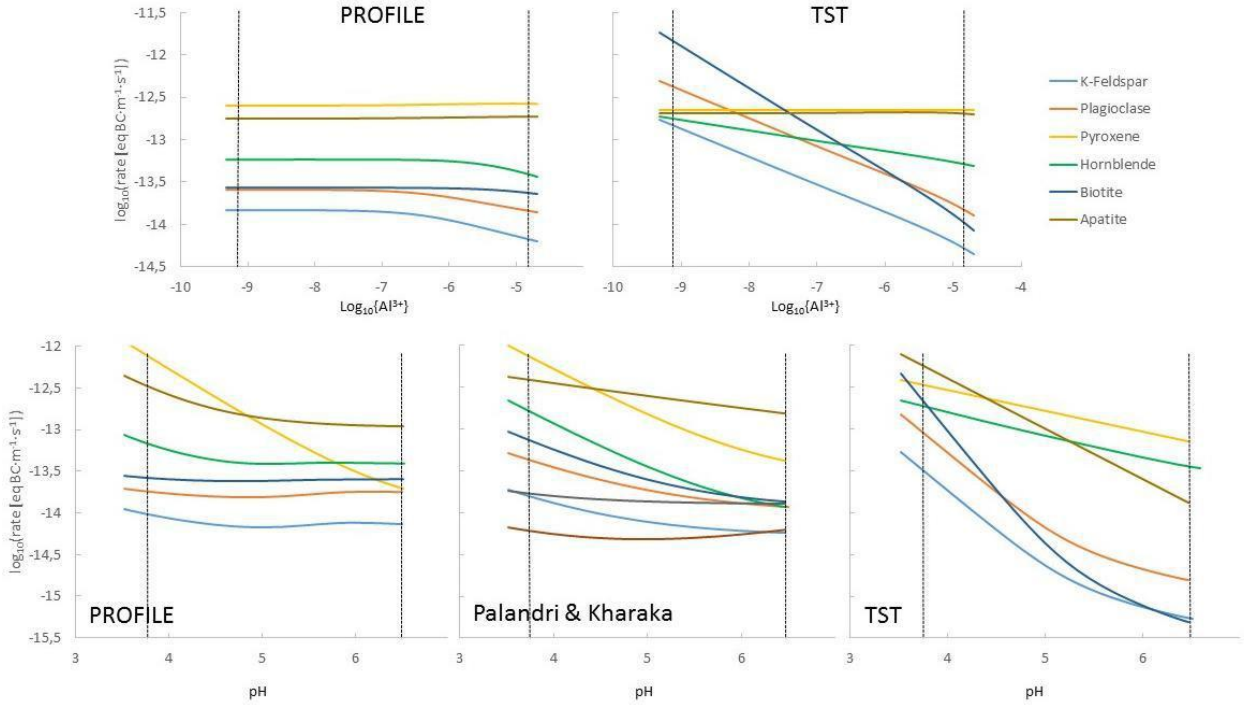

Figure 6: Variation of specific base cation release rates from eight minerals in response to changing aqueous Al^{3+}-activity (upper panel) and pH (lower panel) as calculated from the PROFILE-, the normalized TST-equations and the normalized Palandri & Kharaka-equations. The dashed vertical lines represent the range in aqueous Al^{3+}-activity and pH of the hillslope waters.

4.2 Spatial variability of base cation release rates over the hillslope

We found that significant base cation release occurs along the entire pathway of fluid flow through the hillslope to the stream, even in the last meters of the riparian zone. In particular, the transition zone at S12 is a "hot-spot" for weathering, due to its finer soil texture. The combined contribution of the transition and the riparian zones to total base cation release rate was at least 30 % according to the PROFILE and normalized Palandri & Kharaka models, and at least 20 % according to the normalized TST-model. As the pH is low within the riparian soils, the specific base cation release rates will be relatively high as long as weatherable material is present.

If relatively short hillslopes are considered, riparian zones are likely to contribute significantly to the delivery of weathering products to catchment runoff for three reasons. First, because the riparian zone is

relatively larger for shorter hillslopes, second because most minerals will still be undersaturated in the riparian zone, and finally because the pH is lower than in much of the upslope soils. Of the minerals present at the study site, only K-feldspar was supersaturated anywhere in the hillslope, namely in the deep upslope soil (S12-70, S22-75 and S22-90). In the riparian zone, the lower pH kept K-feldspar undersaturated.

4.3 Uncertainties and simplifications

The base cation fluxes calculated in this study can be compared to the estimates of Ca^{2+} and K^{+}-release rates from chemical weathering from this site presented by Klaminder et al. (2011). The average release rate of Ca^{2+} calculated with seven different approaches was 0.033 (range 0.004-0.15) $eq \cdot yr^{-1} \cdot m^{-2}$, and the average release rate for K^{+} was 0.010 (range 0.002-0.032) $eq \cdot yr^{-1} \cdot m^{-2}$. Of particular interest are the results from previous applications of the PROFILE mode at the study site. Akselsson et al. (2004), using the PROFILE-model, estimated a Ca^{2+}-release rate of 0.016 $eq \cdot yr^{-1} \cdot m^{-2}$ and a K^{+}-release rate of 0.0074 $eq \cdot yr^{-1} \cdot m^{-2}$. In the present study, we calculated a Ca^{2+}-release of 0.032-0.062 and a K^{+}-release of 0.014-0.021 $eq \cdot yr^{-1} \cdot m^{-2}$. Although the most conservative estimate in this study assumes the same depth of the weathering zone, i.e. 1 m, and includes the soil moisture factor of the PROFILE model adopted by Akselsson et al. (2004), the present study included one soil profile with finer texture, i.e. the transition zone, which explains the higher base cation release rates calculated in this study.

The equations used in this study are based on controlled laboratory mineral dissolution experiments, thus exclude factors that may affect rates under field conditions. In particular, direct biological effects are both difficult to quantify and poorly understood. While biological processes (Taylor et al. 2009) notably fungi (Finlay et al. 2010), play a key role in mineral weathering processes, evidence also suggests that soil mycorrhiza (Sverdrup 2010, Smits et al. 2014) as well as humic and fulvic acids (Chin and Mills 1991, Ochs et al. 1993, Oelkers and Schott 1998) have a small or no direct effect on mineral dissolution rates.

The possibility that base cations may be retained by precipitation of secondary phases has not been

599 considered in the present study. However, the most commonly occurring secondary phases in boreal forest
600 soils are imogolite and allophane (Gustafsson et al. 1998), neither of which contain base cations.

601 The accurate calculation of base cation release rates is also confounded by limitations of the mineral
602 dissolution rate models. For example, as K* was not known for most minerals, so the simplified (eq. 10)
603 TST-equation was used rather than its general form (eq. 9); this parameter is potentially important if the
604 mineral is very far from equilibrium, i.e. at low pH or low aqueous Al^{3+}-concentration. For K-feldspar,
605 Gautier et al. (1994) concluded that K* is < $10^{-6.5}$. Using this value in the general TST-equation for K-
606 feldspar dissolution would reduce its dissolution rates up to a factor of 1.8 at the site with the lowest pH,
607 S4-10 cm. However, the total base cation release from K-feldspar of the hillslope was only reduced by a
608 factor of 1.15 when eq. 9 was used. Note also that this calculated value is an upper limit of this difference.

609 The dependence of mineral dissolution rates on chemical affinity at near to equilibrium conditions is also
610 different between the three different mineral dissolution rate models. In the case of PROFILE, rates are
611 assumed to decrease to close to zero near equilibrium by the f_H and f_{H2O}-functions (see eq. 6). However,
612 where K-feldspar was supersaturated, the calculated dissolution rates from PROFILE were still positive,
613 and the f_H and f_{H2O} only slowed dissolution rates by a factor of 1.1. In the PROFILE philosophy, the most
614 accurate way of handling supersaturation would be to let a secondary phase co-precipitate when a mineral
615 is supersaturated (Sverdrup, pers. comm.). However, in this study we set the dissolution rates to zero if a
616 mineral was supersaturated. There are several other aspects and alternative rate laws for the dependence
617 on chemical affinity near equilibrium. Schott et al. (2012) demonstrated that the dissolution rate

dependence on chemical affinity near equilibrium can differ by almost two orders of magnitude, depending on the number of available reactive sites. Moreover, there are likely distinct dissolution mechanisms that dominate for different chemical affinities (Schott et al. 1989). One way of describing this mathematically is to use the parallel rate laws as suggested by Hellmann and Tisserand (2006), where the reaction rate is expressed as the sum of two parallel reactions; one accounting for far-from-equilibrium and one for near-equilibrium dissolution. The calculated retention of base cations is reasonable for Ca^{2+} and Mg^{2+}, but seems unreasonably high for Na^{+} (Table 5, Fig. 2). Considering that Na^{+} is both less biologically active, and has a lower affinity for ion exchange than the divalent cations, the high calculated retention of Na^{+} suggests that the dissolution rates of the main Na^{+}-bearing mineral, i.e. plagioclase, is overestimated in these calculations. Bearing in mind that the PROFILE-model normally is restricted to the unsaturated zone, it is possible that the inhibition from the "brake"-functions (eqs. 6) is too weak when a mineral approaches equilibrium.

In the present study, we chose to explore the uncertainty of three different parameters believed to exert a major influence on the calculated base cation release rates:

1) The depth to the "active weathering zone", which was varied between 1 and 2 m by the water divide. The zero rate depth can be both hydrologically defined, i.e. the depth where the groundwater flow direction becomes parallel rather than perpendicular to the stream, and geochemically defined, i.e. the depth were the net weathering rates become insignificant. As four of six minerals (i.e. hornblende, biotite, pyroxene and apatite) were always highly undersaturated (SI < -11) at the deepest sampled depth of 90 cm, the zero rate depth is more likely to be hydrologically defined at the study site. Preliminary results from an application of the Vertical Equilibrium Model indicates that there the soil is hydrologically inactive at a depth of approximately 3 meters at the water divide.

2) The reactive mineral surface area of the deepest layer of the upslope soil (i.e. S22-90 cm) was varied between 966 and 339 $m^2 \cdot kg^{-1}$ [minerals]. The higher value was calculated from eq. 18 given the measure texture of the soil layer, and deviated considerably from the rest of the S22 profile (Table S2). It is likely that the relationship between reactive surface area and soil texture defined by eq. 18 is not valid for deeper

644 soil layers where the soil is more compacted.

645 3) The inclusion of a soil moisture factor, which is a feature of the PROFILE model and represents the
646 proportion of wetted mineral surface areas. While it is debatable if this factor is physically correct, as in
647 reality all exposed mineral surfaces are always wetted under field conditions, this factor is likely necessary
648 to correctly calculate base cation release rates under field conditions when using the tabulated parameters.

649 Following this reasoning, we conclude that the most likely combination of parameters is: 1) A deep
650 weathering zone, 2) Lower mineral surface area of the deep upslope soil (S22-90 cm), and 3) Including the
651 soil moisture factor. This combination (model 4 in Table S10) would give a total base cation release of
652 0.22 eq[BC]·yr^{-1}·m^{-2} [soil surface], and a calculated retention of 44 % for Ca^{2+}, 54 % for Mg^{2+}, 79 % for
653 Na^{+} and 81 % for K^{+}. Furthermore, the distribution of base cation release between the soil zones becomes:
654 6.1-10.8 % from the riparian zone, 17-30 % from the transition zone, and 61-77 % from the upslope zone.
655 In terms of the relative contribution from the unsaturated versus the saturated zones, the contribution from
656 the former was 39-55 %, and from the latter 45-61 %.

657

658 **4.4 Conclusions and recommendations**

659 This study investigated the significance of varying soil water chemistry and choice of mineral dissolution
660 rate equations of the calculated base cation release rates in different parts of a hillslope. Although

aluminum, DOC and carbon dioxide play different roles in the three models, it is the variation of calculated rates with pH that is the most important factor influencing the calculated base cation release rates – or in the case of the TST rate-equations, the balance between pH and aqueous Al^{3+}-concentration.

By using soil water chemistry data measured as a function of time and space, this study provides insight into weathering rates at a catchment scale. Such insight is required to assess how forest management will be affected by the base cation supply to catchment runoff, with its implications for the vulnerability of aquatic ecosystems to change in areas where surface pH and Al-toxicity can be strongly influenced by relatively small changes in base cation delivery. We have demonstrated that a considerable uncertainty in model calculations stems from differences in the kinetic description of mineral dissolution. However, for the spatial variability, much of this uncertainty was overridden by heterogeneities of the soil texture. We have also demonstrated that for the relatively short hillslope lengths considered here, the riparian and transition zones are significant contributors to the base cation delivery to runoff, partly because the low pH enhances the weathering rates.

Acknowledgements

We thank the Krycklan Catchment Study for excellent field data.

Funding: This work was supported by the FORMAS Strong Research Environment Quantifying WeAthering RaTes for Sustainable Forestry (QWARTS), Contract 2011-1691.

References

Aagard, P. and H. C. Helgeson, 1982. Thermodynamic and kinetic constraints on reaction rates among minerals and aqueous solutions: I. Theoretical considerations. Amer. J. Sci. 282 237-285.

Akselsson, C., J. Holmqvist, M. Alveteg, D. Kurz and H. Sverdrup, 2004. Scaling andmapping regional calculation of soil chemical weathering rates in Sweden. Water Air Soil Pollut.: Focus 4 671–681.

Akselsson, C., O. Westling, H. Sverdrup and P. Gundersen, 2007a. Nutrient and carbon budgets in forest

686 soils as decision support in sustainable forest management. Forest Ecol Manag 238(1-3), 167-174.

687 Akselsson, C., O. Westling, H. Sverdrup, J. Holmqvist, G. Thelin, E. Uggla and G. Malm, 2007b. Impact
688 of harvest intensity on long-term base cation budgets in Swedish forest soils. Water, Air, Soil Pollut:
689 Focus 7(1-3), 201-210.

690 Amvrosiadi, N., K. Bishop, T. Grabs, K. Beven and J. Seibert, 2016. Water Storage Dynamics in a till
691 hillslope: The foundation for modeling flows and residence times. Submitted.

692 Ball, J. W. and D. K. Nordstrom, 1991. WATEQ4F-User's manual. U.S., Geological Survey.

693 Blum, J. D., A. Klaue, C. A. Nezat, C. T. Driscoll, C. E. Johnson, T. G. Siccama, C. Eagar, T. J. Fahey
694 and G. E. Likens, 2002. Mycorrhizal weathering of apatite as an important calcium source in base-poor
695 forest ecosystems. Nature 417(6890), 729-731. Doi 10.1038/Nature00793.

696 Brantley, S. L., 1992. Kinetics of dissolution and precipitation-experimental and field results. Water–Rock
697 Interaction 7 465-469.

698 Chin, P. K. F. and G. L. Mills, 1991. Kinetics and Mechanisms of Kaolinite Dissolution - Effects of
699 Organic-Ligands. Chem Geol 90(3-4), 307-317.

700 Cory, N., H. Laudon, S. Köhler, J. Seibert and K. Bishop, 2007. Evolution of soil solution aluminum
701 during transport along a forested boreal hillslope. J Geophys Res-Biogeo 112(G3). Artn
702 G0301410.1029/2006jg000387.

703 Cosby, B. J., R. C. Ferrier, A. Jenkins and R. F. Wright, 2001. Modelling the effects of acid deposition:
704 refinements, adjustments and inclusion of nitrogen dynamics in the MAGIC model. Modelling the effects
705 of acid deposition: refinements, adjustments and inclusion of nitrogen dynamics in the MAGIC model.
706 5(3) 499-518.

707 Finlay, R., H. Wallander, M. M. Smits, S. Holmström, P. Van Hees, B. Lian and A. Rosling, 2010. The
708 role of fungi in biogenic weathering in boreal forest soils. Fungal Biol Rev 23(4) 101-106.

709 Frogner, P. and P. Schweda, 1998. Hornblende dissolution kinetics at 25 degrees C. Chem Geol 151(1-4),
710 169-179.

711 Futter, M. N., S. Valinia, S. Löfgren, S. J. Köhler and J. Fölster, 2014. Long-term trends in water
712 chemistry of acid-sensitive Swedish lakes show slow recovery from historic acidification. Ambio 43 77-
713 90. 10.1007/s13280-014-0563-2.

714 Gautier, J. M., E. H. Oelkers and J. Schott, 1994. Experimental-Study of K-Feldspar Dissolution Rates as
715 a Function of Chemical Affinity at 150-Degrees-C and Ph-9. Geochim Cosmochim Ac 58(21), 4549-
716 4560.

717 Gerard, F., K. U. Mayer, M. J. Hodson and J. Ranger, 2008. Modelling the biogeochemical cycle of
718 silicon in soils: Application to a temperate forest ecosystem. Geochim Cosmochim Ac 72(3), 741-758.
719 10.1016/j.gca.2007.11.010.

720 Godderis, Y., L. M. Francois, A. Probst, J. Schott, D. Moncoulon, D. Labat and D. Viville, 2006.
721 Modelling weathering processes at the catchment scale: The WITCH numerical model. Geochim
722 Cosmochim Ac 70(5), 1128-1147. 10.1016/j.gca.2005.11.018.

723 Golubev, S. V., O. S. Pokrovsky and J. Schott, 2005. Experimental determination of the effect of

724 dissolved CO2 on the dissolution kinetics of Mg and Ca silicates at 25 degrees C. Chem Geol 217(3-4),
725 227-238.

726 Gustafsson, J. P., E. Karltun and P. Bhattacharya, 1998. Allophane and imogolite in Swedish soils.
727 Division of Land and Water Resources, Department of Civil and Environmental Engineering, Royal
728 Institute of Technology (KTH).

729 Harouiya, N., C. Chairat, S. J. Kohler, R. Gout and E. H. Oelkers, 2007. The dissolution kinetics and
730 apparent solubility of natural apatite in closed reactors at temperatures from 5 to 50 degrees C and pH
731 from 1 to 6. Chem Geol 244(3-4), 554-568.

732 Hellmann, R. and D. Tisserand, 2006. Dissolution kinetics as a function of the Gibbs free energy of
733 reaction: An experimental study based on albite feldspar. Geochim Cosmochim Ac 70(2), 364-383.

734 Iwald, J., S. Löfgren, J. Stendahl and E. Karltun, 2013. Acidifying effect of removal of tree stumps and
735 logging residues as compared to atmospheric deposition. Forest Ecol Manag 290 49-58.
736 10.1016/j.foreco.2012.06.022.

737 Johnson, J., G. Anderson and D. L. Parkhurst, 2000. Database “thermo.com.V8.R6.230”. Rev. 1.11.,

738 Klaminder, J., R. W. Lucas, M. N. Futter, K. H. Bishop, S. J. Köhler, G. Egnell and H. Laudon, 2011.
739 Silicate mineral weathering rate estimates: Are they precise enough to be useful when predicting the
740 recovery of nutrient pools after harvesting? Forest Ecol Manag 261(1), 1-9.

741 Lasaga, A. C., 1981. Transition State Theory. Rev. Miner. 8 135–169.

742 Laudon, H., I. Taberman, A. Ågren, M. Futter, M. Ottosson-Löfvenius and K. Bishop, 2013. The
743 Krycklan Catchment Study-A flagship infrastructure for hydrology, biogeochemistry, and climate research
744 in the boreal landscape. Water Resour Res 49(10), 7154-7158. 10.1002/wrcr.20520.

745 Ledesma, J., T. Grabs, M. Futter, K. Bishop, H. Laudon and S. Köhler, 2013. Riparian zone control on
746 base cation concentration in boreal streams. Biogeosciences 10(6), 3849-3868.

747 Leith, F. I., K. J. Dinsmore, M. B. Wallin, M. F. Billett, K. V. Heal, H. Laudon, M. G. Öquist and K.
748 Bishop, 2015. Carbon dioxide transport across the hillslope-riparian-stream continuum in a boreal
749 headwater catchment. Biogeosciences 12(6), 1881-1892.

750 Magnusson, T., 1989. A method for equilibration chamber sampling and gas chromatographic analysis of
751 the soil atmosphere. Plant and Soil 120 39-47.

752 Miskovsky, K., 1987. Mineralogiska studier av utvalda moränsekvenser - en studie av Svartberget i
753 Vindeln. Department of Public Health, Umeå University.

754 Ochs, M., B. I, W. Stumm and B. Cosovic, 1993. Effects of Root Exudates and Humic Substances on
755 Weathering Kinetics. Water Air Soil Poll 68(1-2), 213-229.

756 Oelkers, E. H., J. Schott and J. L. Devidal, 1994. The Effect of Aluminum, Ph, and Chemical Affinity on
757 the Rates of Aluminosilicate Dissolution Reactions. Geochim Cosmochim Ac 58(9), 2011-2024. Doi
758 10.1016/0016-7037(94)90281-X.

759 Oelkers, E. H. and J. Schott, 1998. Does organic acid adsorption affect alkali-feldspar dissolution rates?
760 Chem Geol 151(1-4), 235-245.

761 Oelkers, E. H., 2001. General kinetic description of multioxide silicate mineral and glass dissolution.
762 Geochim Cosmochim Ac 65(21), 3703-3719. Doi 10.1016/S0016-7037(01)00710-4.

763 Oelkers, E. H. and J. Schott, 2001. An experimental study of enstatite dissolution rates as a function of
764 pH, temperature, and aqueous Mg and Si concentration, and the mechanism of pyroxene/pyroxenoid
765 dissolution. Geochim Cosmochim Ac 65(8), 1219-1231.

766 Oelkers, E. H., J. Schott, J. M. Gauthier and T. Herrero-Roncal, 2008. An experimental study of the
767 dissolution mechanism and rates of muscovite. Geochim Cosmochim Ac 72(20), 4948-4961.

768 Oni, S. K., M. N. Futter, K. Bishop, S. J. Köhler, M. Ottosson-Löfvenius and H. Laudon, 2013. Long-term
769 patterns in dissolved organic carbon, major elements and trace metals in boreal headwater catchments:
770 trends, mechanisms and heterogeneity. Biogeosciences 10(4), 2315-2330. 10.5194/bg-10-2315-2013.

771 Palandri, J. L. and Y. K. Kharaka, 2004. A compilation of rate parameters of water-mineral interaction
772 kinetics for application to geochemical modeling. Geological Survey, Menlo Park, CA.

773 Schnoor, J. L., 1990. Kinetics of chemical weathering: a comparison of laboratory and field weathering
774 rates. Aquatic Chemical Kinetics: Reaction Rates of Processes in Natural Waters. Environmental Science
775 and Technology Series, John Wiley & Sons, New York.**:** 475-504.

776 Schott, J., S. Brantley, D. Crerar, C. Guy, M. Borcsik and C. Willaime, 1989. Dissolution Kinetics of
777 Strained Calcite. Geochim Cosmochim Ac 53(2), 373-382.

778 Schott, J., O. S. Pokrovsky and E. H. Oelkers, 2009. The Link Between Mineral Dissolution/Precipitation
779 Kinetics and Solution Chemistry. Rev Mineral Geochem 70 207-258. 10.2138/rmg.2009.70.6.

780 Schott, J., E. H. Oelkers, P. Benezeth, Y. Godderis and L. Francois, 2012. Can accurate kinetic laws be
781 created to describe chemical weathering? Cr Geosci 344(11-12), 568-585.

782 Sjöstedt, C. S., J. P. Gustafsson and S. J. Köhler, 2010. Chemical Equilibrium Modeling of Organic Acids,
783 pH, Aluminum, and Iron in Swedish Surface Waters. Environ. Sci. Technol. 44(22), 8587-8593.

784 Smits, M. M., L. Johansson and H. Wallander, 2014. Soil fungi appear to have a retarding rather than a
785 stimulating role on soil apatite weathering. Plant Soil 385(1-2), 217-228.

786 Sverdrup, H., 1990. The Kinetics of Base Cation Release Due to Chemical Weathering, Lund University.

787 Sverdrup, H. and P. Warfvinge, 1993. Calculating Field Weathering Rates Using a Mechanistic
788 Geochemical Model Profile. Appl Geochem 8(3), 273-283. Doi 10.1016/0883-2927(93)90042-F.

789 Sverdrup, H. and P. Warfvinge, 1995. Critical loads of acidity for Swedish forest ecosystems. Ecol Bull
790 75-89.

791 Sverdrup, H., P. Warfvinge and K. Rosén, 1995. Critical loads of acidity and nitrogen, based on multiple
792 criteria for different Swedish ecosystems. Water Air Soil Poll 85(4), 2375-2380.

793 Sverdrup, H., 1996. Geochemistry, the key to understanding environmental chemistry. Sci Total Environ
794 183(1-2), 67-87.

795 Sverdrup, H. and K. Rosén, 1998. Long-term base cation mass balances for Swedish forests and the
796 concept of sustainability. Forest Ecol Manag 110(1-3), 221-236.

Sverdrup, H., 2010. Chemical weathering of soil minerals and the role of biological processes. Fungal Biology Reviews 23(4) 94-100.

Taylor, A. S., J. D. Blum, A. C. Lasaga and I. N. MacInnes, 1999. Kinetics of dissolution and Sr release during biotite and phlogopite weathering. Geochim Cosmochim Ac 64(7), 1191-1208.

Taylor, L. L., J. R. Leake, J. Quirk, K. Hardy, S. A. Banwart and D. J. Beerling, 2009. Biological weathering and the long-term carbon cycle: integrating mycorrhizal evolution and function into the current paradigm. Geobiology 7(2), 171-191.

Tipping, E. and M. A. Hurley, 1992. A Unifying Model of Cation Binding by Humic Substances. Geochim Cosmochim Ac 56(10), 3627-3641.

Todorov, T., D. Rabadjieva and S. Tepavitcharova, 2006. New thermodynamic database for more precise simulation of metal species in natural waters. Journal of the University of Chemical Technology and Metallurgy 41(1), 97-102.

Warfvinge, P. and H. Sverdrup, 1992. Calculating Critical Loads of Acid Deposition with Profile - a Steady-State Soil Chemistry Model. Water Air Soil Poll 63(1-2), 119-143. Doi 10.1007/Bf00475626.

Warfvinge, P. and H. Sverdrup, 1995. Critical loads of acidity to Swedish forest soils: methods, data and results. D. o. C. Engineering, Lund University.

Zetterberg, T., S. J. Kohler and S. Lofgren, 2014. Sensitivity analyses of MAGIC modelled predictions of future impacts of whole-tree harvest on soil calcium supply and stream acid neutralizing capacity 494-495 187-201. 10.1016/j.scitotenv.2014.06.114.

Supplementary information for online publication only

Click here to download Background dataset for online publication only: Supplementary information II.docx